Navigating Complex Labyrinths: Optimal Paths from Chemical Waves

Oliver Steinbock, Agota Toth, Kenneth Showalter

Science, New Series, Volume 267, Issue 5199 (Feb. 10, 1995), 868-871.

Stable URL:
http://links.jstor.org/sici?sici=0036-8075%2819950210%293%3A267%3A5199%3C868%3ANCLOPF%3E2.0.CO%3B2-T

Navigating Complex Labyrinths: Optimal Paths from Chemical Waves

Oliver Steinbock, Ágota Tóth, Kenneth Showalter*

The properties of excitable media are exploited to find minimum-length paths in complex labyrinths. Optimal pathways are experimentally determined by the collection of time-lapse position information on chemical waves propagating through mazes prepared with the Belousov-Zhabotinsky reaction. The corresponding velocity fields provide maps of optimal paths from every point in an image grid to a particular target point. Collisions of waves that were temporarily separated by obstacles mark boundary lines between significantly different paths with the same absolute distance. The pathfinding algorithm is tested in very complex mazes with a simple reaction-diffusion model.

Propagating waves in spatially distributed, excitable media arise from the coupling of a positive feedback process with some form of transport, for example, autocatalytic chemical reaction with molecular diffusion (*1*). Such waves are observed in biological (*2*), chemical (*3*), and physicochemical (*4*) systems and typically exhibit constant velocities and annihilation in collisions with boundaries or other waves (*5*, *6*). In this report we describe how these features give rise to a highly efficient algorithm for the determination of optimal paths. Conventional pathfinding methods typically rely on iterative searches, in which all possible pathways between a point of interest and a target point are successively determined and the optimal path is then selected (*7*). In an excitable medium, a single propagating wave generates a map for the optimal path from every point of the system to a target point. This feature was first noted by Sepulchre *et al.* (*8*) in a computational study of wave propagation in an oscillatory medium containing impenetrable obstacles.

Experimental studies of wave propagation in complex labyrinths were carried out with the excitable Belousov-Zhabotinsky (BZ) reaction (*9*) by means of time-lapse digital imaging techniques. Planar labyrinths were made of vinyl-acrylic membranes saturated with BZ reaction mixture (*10*). We prepared impenetrable barriers by carefully cutting out rectangular regions of the membrane. This simple procedure allowed the realization of a variety of geometries and provided an effectively two-dimensional system without hydrodynamic disturbances. The composition of the BZ solution was prepared so that no spontaneous wave initiations occurred; however, waves could be reproducibly initiated by allowing a silver wire to contact the reagent-loaded membrane. The wave propagation was monitored by image analysis of monochromatic light (wavelength $\lambda = 500$ nm) reflected from the medium. The video signals were recorded and then digitized into image sequences (*11*), which were enhanced with standard imaging routines and analyzed.

Figure 1A shows a 50-frame composite image of a chemical wave propagating through a BZ-membrane labyrinth. The wave splits at each junction during its propagation and therefore reaches all points in the maze that are connected to the starting point (at the lower left corner). Wave segments that propagate into blind channels ultimately vanish on collision with the boundaries. Each snapshot shows waves at an equal distance from their positions in the previous snapshot, given by the product of the constant velocity (2.41 ± 0.18 mm/min) and the time between each two snapshots (50 s). To a good approximation, waves propagate according to Huygens's principle, where the front advances a fixed distance per unit of time in a direction normal to the front. The effects of curvature on the wave velocity (*12*), to be discussed below, are slight for mazes with sufficiently large length scales as considered here.

Image sequences with higher temporal resolution allow the generation of maps that give the path length from any location in the maze to a given target point, within the resolution of the composite image. Figure 1B shows a color-coded distance map based on higher resolution data, where the colors are keyed to the elapsed time from the wave initiation to the local maximum of excitation at each point. The minimum path length from any point in the maze to the target point S is given by the product of the elapsed time assigned to that point and the constant wave velocity. The optimal transit time and distance for every location in the labyrinth are determined by a single propagating wave, representing a highly efficient accumulation of information in a parallel manner.

The space-time information compiled in Fig. 1B provides the basis for a determination of detailed minimum-length paths. The optimal path from any arbitrary point to the target point is easily determined according to the velocity field, which is generated by specifying the direction of wave propagation at each point in the grid. The vector field derived from Fig. 1B is shown in Fig. 1C, along with several examples of optimal paths. One can compute the specific shortest path connections from the time-indexed points of the composite image by searching for the nearest point indexed $t - \tau$, where t is the elapsed time from the wave initiation to the current position and τ is the time increment between successive images.

Figure 1C shows that the path optimization includes local features such as diagonal trajectories in the corridors of the labyrinth. The labyrinth is therefore analyzed as a two-dimensional array of rectangular segments rather than as a mesh of one-dimensional strings. Path boundaries, created by colliding waves that previously had been separated by barriers, are also defined (see Fig. 1B). These boundaries demarcate significantly different pathways of equal distance to the target point S. The maze is consequently divided into local domains that correspond to families of pathways, where paths in one domain are matched by different paths of equal length in another domain.

Distinct basins of attraction arise from the synchronous initiation of several waves at different locations in a maze. In contrast to experiments with a single initiation, two different types of annihilation loci occur: path boundaries from waves originating at a single initiation point and collision boundaries from waves originating at different initiation points. The latter represent boundaries composed of points that are equidistant to two initiation sites; the intersection of three or more boundaries defines points equidistant to each of the corresponding initiation sites. Both types of boundaries are shown in Fig. 2, in which four waves were initiated almost synchronously at sites S1, S2, S3, and S4 near the corners of the maze.

The basin of attraction associated with each initiation site is shown by a single color in Fig. 2, where the intensity is indexed to the elapsed time from the wave initiation. Each color boundary represents a separatrix between two basins. In terms of a potential surface description, the minimum of each basin lies at the wave initiation point and the height at any point on the surrounding surface is proportional to the elapsed time assigned to that point. Each separatrix is defined by the locus of collision times and represents a "watershed" separating trajectories that lead to different target points.

Department of Chemistry, West Virginia University, Morgantown, WV 26506, USA.

*To whom correspondence should be addressed.

Examples of shortest distance paths are also shown in Fig. 2, computed by tracking nearest $t - \tau$ points as described above. Four initial points chosen near the intersection of the S1, S2, and S3 basins at $(x, y) =$ (14 mm, 16 mm) lead to three different target points with two significantly different paths to S2. Three other paths are also shown, with initial points chosen to be near a path boundary and a basin separatrix.

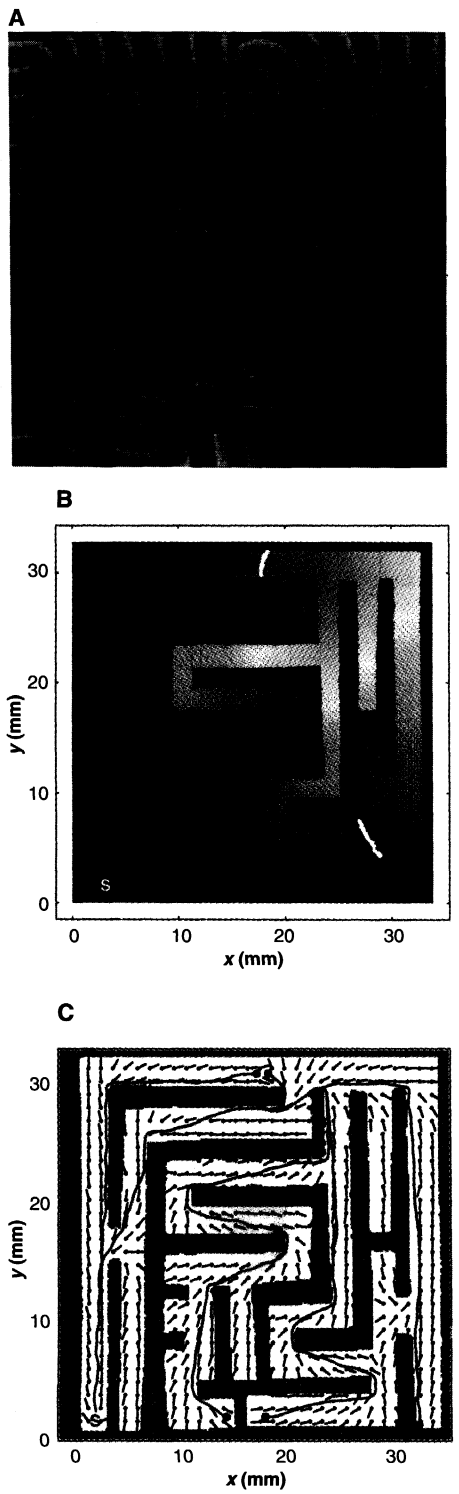

Fig. 1. (**A**) Chemical wave propagating through a BZ membrane labyrinth. A sequence of 50 images obtained at 50-s intervals was superimposed to form the composite image. The wave was initiated in the lower left corner of the maze. The total area of the maze is 3.2 cm by 3.2 cm, with obstacles appearing as black rectangular segments. (**B**) Color map representing the time difference between wave initiation and local excitation for all points in the labyrinth. A sequence of 250 images obtained at 10-s intervals was used to form the time-indexed composite image (yielding a spacing of ~4 pixels between successive front positions). Red, green, yellow, and blue correspond to successively longer times over the total elapsed time of 2500 s. White lines show path boundaries. (**C**) Velocity field describing the local wave propagation direction. Small black dots represent the origins of vectors. The shortest paths between five points and the target point S are shown in red.

While propagating chemical waves provide vivid examples of path optimization in excitable media, computational simulations of such waves allow the approach to be demonstrated in very complex labyrinths. We use a generic model for excitable media, the two-variable Barkley model (*13*), which has the form

$$\frac{\partial u}{\partial t} = \nabla^2 u + f(u, v) \quad (1)$$

$$\frac{\partial v}{\partial t} = g(u, v) \quad (2)$$

where the variables u and v describe the spatiotemporal dynamics of a propagator species and a controller species, respectively (*14*).

Figure 3 shows the results of simulated wave propagation through a complex labyrinth that was developed in 1664 by G. A. Boeckler (*15*). As in the experiments, the color coding corresponds to transit times for the shortest length path from any point to the target point, the red door at the top boundary where the wave was initiated. The color map shows very different transit times for points in each of the four square areas and the central circular area. The map indicates times only for the optimal paths (in fact, there are multiple paths from any particular starting point to the target point). An example of an optimal path originating from the lower left square (colored blue) is shown by the white dashed line. This trajectory was computed from the time-indexed points according to the procedure described above. Visual inspection of the labyrinth reveals another, significantly different pathway, which exceeds the optimal path in length by only 7%. We also carried out an additional calculation to prove that the optimal, shortest length path is unaffected by switching the point of origin with the target point and vice versa. The optimal path obtained from this "reverse" calculation is the same as that shown in Fig. 3.

Throughout this report we have assumed constant-velocity waves propagating according to Huygens's principle. This assumption is the basis of the vector fields derived from the time-indexed grids and the $t - \tau$ algorithm for determining optimal paths. In fact, front curvature may significantly affect the velocity of wave propagation (*12*). The error introduced by neglecting curvature effects is small in the optimal

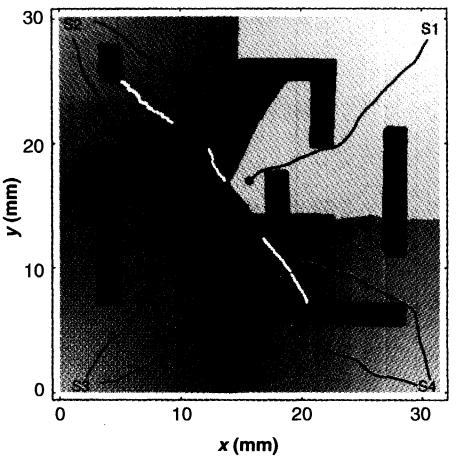

Fig. 2. Color map showing a BZ membrane labyrinth in which four waves were initiated almost synchronously (~5-s intervals) at S1, S2, S3, and S4. The area covered by each wave is distinguished by a different color, with the color intensity at any point proportional to the time elapsed since wave initiation. Obstacles are plotted in black, and the shortest paths between seven points and various target points are shown in red. The total duration of the experiment was ~450 s.

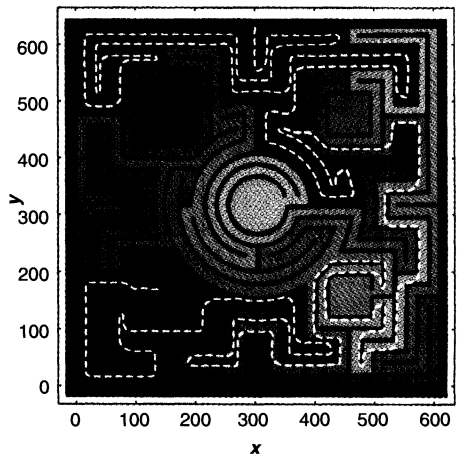

Fig. 3. Interrogation of a complex labyrinth by wave propagation in the Barkley model (*13, 14*). Colors indicate propagation times for a wave that was initiated at the entrance, shown in red at the top boundary of the maze. The color coding is the same as in Fig. 1 over a total elapsed (dimensionless) time of 1174.15. The dashed white line shows the shortest path from the lower left square region (blue) to the maze entrance (red).

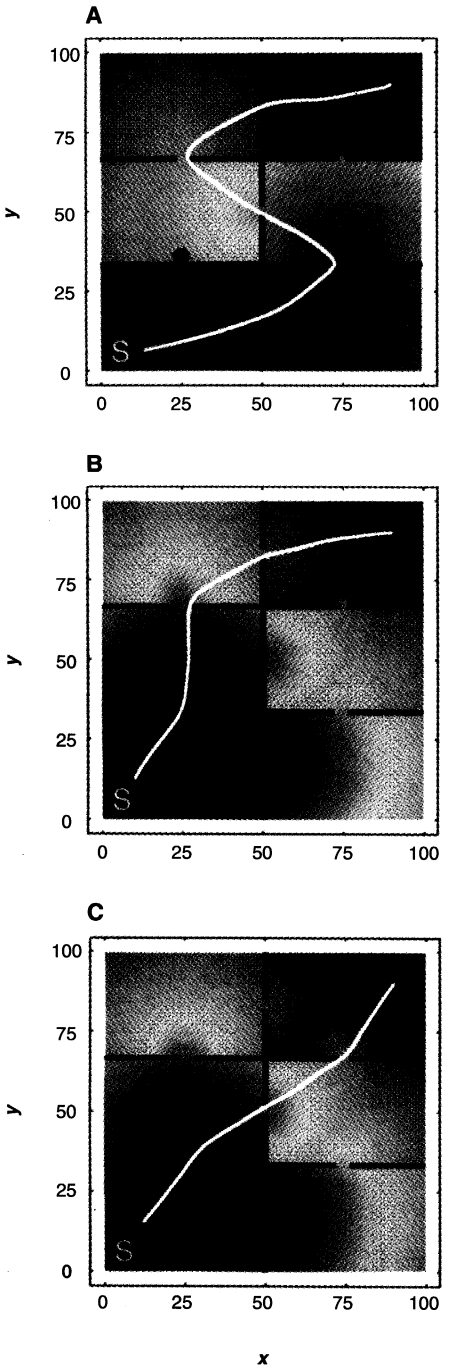

Fig. 4. Interrogation of "door size" in a labyrinth with narrow passages between barriers by wave propagation in the Barkley model (*13, 14*). Distance map and optimal trajectory (white) generated by medium with low excitability, $a = 0.50$, $r_c = 1.125$ (**A**); intermediate excitability, $a = 0.70$, $r_c = 0.825$ (**B**); high excitability, $a = 0.85$, $r_c = 0.675$ (**C**). The color coding is the same as in Fig. 1 over a total elapsed (dimensionless) time of 24.15 (A), 15.83 (B), and 14.60 (C). Door sizes [r = channel radius, (x, y) = maze coordinates]: $r = 1.35$, $(x, y) = (50, 16.5)$; $r = 1.05$, $(x, y) = (25, 33)$; $r = 1.35$, $(x, y) = (75, 33)$; $r = 1.35$, $(x, y) = (50, 50)$; $r = 1.35$, $(x, y) = (25, 66)$; $r = 0.75$, $(x, y) = (75, 66)$; $r = 1.35$, $(x, y) = (50, 83.5)$. The integration was carried out on a grid of 300 points by 300 points (grid spacing $\Delta x = 0.33$, time step $\Delta t = 0.0056$) with the parameters $b = 0.01$, $\epsilon = 0.02$, and a indicated above.

paths above; however, errors in the transit times may become significant in mazes with smaller length scales.

Curvature effects considered in a general context can be exploited to extend the pathfinding capabilities of excitable media. The dependence of wave velocity on curvature allows the determination of "door size" in complex labyrinths with narrow gaps between barriers. The velocity depends on front curvature according to an eikonal relation (*12*): $c = c_0 + D\kappa$, where c is the normal wave velocity, c_0 is the planar wave velocity, D is the diffusion coefficient of the autocatalyst, and κ is the curvature of the front. For convex waves ($\kappa < 0$), such as those exiting narrow channels, the propagation velocity is reduced by the enhanced dispersion of the autocatalyst. A critical nucleation size with a radius of curvature ($r = 1/|\kappa|$) given by $r_c = D/c_0$ is predicted when the normal velocity is reduced to zero. Thus, as c_0 is decreased, r_c increases and channels with radii below r_c do not allow waves to pass. Recent experiments with BZ waves propagating through microcapillary tubes have demonstrated this behavior (*16*).

Figure 4 shows a labyrinth in which waves calculated with the Barkley model were used to determine the relative channel widths between obstacles. Color maps generated from low-, medium-, and high-velocity waves are shown in Fig. 4, A through C, respectively. For the slowest wave (Fig. 4A), all but two channels have $r > r_c$. Because two of the "doors" are too small, the optimal trajectory from the starting point in the upper right corner to the target point S takes a circuitous route through the "allowed" openings. Above a critical velocity, the opening at $(x, y) = (25, 33)$ becomes available for wave propagation (because $r > r_c$) and a more direct path to the target point S is determined (Fig. 4B). For the fastest wave, the opening at $(x, y) = (75, 66)$ allows wave propagation and a nearly diagonal pathway is determined (Fig. 4C). Thus, optimal paths are determined even when some openings are too small, and the sizes of the openings can be found by variation of wave propagation velocity.

Propagating waves in excitable media provide an interesting, and potentially useful, alternative to traditional iterative-search methods for determining optimal paths. A relatively simple analysis provides optimal paths from every point in a grid to a target point. Thus, a robot in a large warehouse could readily use such a map at any point without needing to recompute its trajectory at each new location to deliver a parcel to loading dock S. The method can easily accommodate changing labyrinths as well, provided that the time scale for the changes is longer than the time required for recomputing the vector field. In addition, the method automatically discerns which doors are wide enough for the parcel, providing an optimal trajectory that ignores any doors that are too small.

While the computational implementation of the reaction-diffusion algorithm provides intriguing possibilities for practical applications, the experimental results point to possible mechanisms for optimization in biological systems. Neural pathways, for example, are known to be extremely complex, yet highly efficient (*17*). Could path optimization in networks of neurons rely on the properties of excitable media, as suggested in the optimal path determinations presented here? This intriguing possibility provides, in itself, ample reason to develop an understanding of optimization capabilities of excitable media. We believe that the experimental approach could also be transferred to microscopic reaction-diffusion systems, such as the oxidation of carbon monoxide on platinum (*4*). Waves interacting with complex boundaries created by photolithography have been recently studied with the use of this system (*18*), suggesting that path optimization could be readily implemented on a microscopic scale.

REFERENCES AND NOTES

1. A. T. Winfree, *The Geometry of Biological Time* (Springer, Berlin, 1980); J. Ross, S. C. Müller, C. Vidal, *Science* **240**, 460 (1988).
2. J. M. Davidenko, A. M. Pertsov, R. Salomonsz, W. Baxter, J. Jalife, *Nature* **355**, 349 (1992); A. Gorelova and J. Bures, *J. Neurobiol.* **14**, 353 (1983); J. Lechleiter, S. Girard, E. Peralta, D. Clapham, *Science* **252**, 123 (1991).
3. R. J. Field and M. Burger, Eds., *Oscillations and Traveling Waves in Chemical Systems* (Wiley, New York, 1985); A. T. Winfree, *Science* **175**, 634 (1972).
4. H. H. Rotermund, S. Jakubith, A. von Oertzen, G. Ertl, *Phys. Rev. Lett.* **66**, 3083 (1991).
5. A. S. Mikhailov, *Foundation of Synergetics I: Distributed Active Systems* (Springer, Berlin, 1990).
6. Reflection of waves colliding with no-flux boundaries and with other waves has been recently reported in a model reaction-diffusion system [W. N. Reynolds, J. E. Pearson, S. Ponce-Dawson, *Phys. Rev. Lett.* **72**, 2797 (1994); V. Petrov, S. K. Scott, K. Showalter, *Philos. Trans. R. Soc. London Ser. A* **443**, 631 (1994)].
7. P. A. Steenbrink, *Optimization of Transport Networks* (Wiley, London, 1974); R. Gould, *Graph Theory* (Benjamin-Cummings, Menlo Park, CA, 1988); J. Malkevitch and W. Meyer, *Graphs, Models, and Finite Mathematics* (Prentice-Hall, Englewood Cliffs, NJ, 1974).
8. J. A. Sepulchre, A. Babloyantz, L. Steels, in *Proceedings of the International Conference on Artificial Neural Networks*, T. Kohonen, K. Makisara, O. Simula, J. Kangas, Eds. (Elsevier, Amsterdam, 1991), pp. 1265–1268.
9. A. N. Zaikin and A. M. Zhabotinsky, *Nature* **225**, 535 (1970).
10. Cut membranes (Gelman Metricel; thickness, 140 μm; pore size, 0.45 μm) were soaked with BZ solution and covered with silicone oil in a thermostated petri dish maintained at 25.0° ± 0.2°C. Initial reagent concentrations were as follows: $[NaBrO_3] = 0.2$ M, $[H_2SO_4] = 0.4$ M, [malonic acid] = 0.17 M, [NaBr] = 0.1 M, [ferroin] = 1.0 mM.
11. S. C. Müller, Th. Plesser, B. Hess, *Physica D* **24**, 71 (1987).
12. J. J. Tyson and J. P. Keener, *ibid.* **32**, 327 (1988); V.

S. Zykov, *Biophysics* **25**, 906 (1980).
13. D. Barkley, *Physica D* **49**, 61 (1991).
14. The functions f and g are defined as $f(u, v) = (1/\epsilon)u(1 - u)[u - (v + b)/a]$ and $g(u, v) = u - v$. The parameter values $a = 0.9$, $b = 0.05$, and $\epsilon = 0.02$ were chosen to model an excitable system. The equations were integrated on a grid of 480 points by 480 points (grid spacing $\Delta x = 1.3$, time step $\Delta t = 0.085$) with the Laplacian operator ∇^2 approximated by a standard nine-point formula. (The same optimal path was found in a higher resolution calculation with grid spacing $\Delta x = 0.65$ and time step $\Delta t = 0.011$.) We were able to realize different complex labyrinths by digitizing corresponding line drawings and modeling the borders and obstacles as regions with constant, steady-state values of u and v. These boundary conditions correspond to "sink" boundaries and reflect the experimental system, where all edges of the membrane were in contact with silicone oil.
15. W. H. Matthews, *Mazes and Labyrinths* (Longmans, London, 1922).
16. Á. Tóth, V. Gáspár, K. Showalter, *J. Phys. Chem.* **98**, 522 (1994).
17. E. R. Kandel, J. H. Schwartz, T. M. Jessell, *Principles of Neural Science* (Elsevier, New York, ed. 3, 1991).
18. M. D. Graham *et al.*, *Science* **264**, 80 (1994).
19. This research was supported by the National Science Foundation (grant CHE-9222616). We acknowledge the donors of the Petroleum Research Fund, administered by the American Chemical Society, for partial support of this research.

26 August 1994; accepted 10 November 1994

Electrochemical Detection of Single Molecules

Fu-Ren F. Fan and Allen J. Bard*

The electrochemical behavior of a single molecule can be observed by trapping a small volume of a dilute solution of the electroactive species between an ultramicroelectrode tip with a diameter of ~15 nanometers and a conductive substrate. A scanning electrochemical microscope was used to adjust the tip-substrate distance (~10 nanometers), and the oxidation of [(trimethylammonio)methyl] ferrocene (Cp_2FeTMA^+) to Cp_2FeTMA^{2+} was carried out. The response was stochastic, and anodic current peaks were observed as the molecule moved into and out of the electrode-substrate gap. Similar experiments were performed with a solution containing two redox species, ferrocene carboxylate (Cp_2FeCOO^-) and $Os(bpy)_3^{2+}$ (bpy is 2,2′-bipyridyl).

A number of techniques have been used in recent years to detect single molecules or ions in different environments. These include the detection of ions that are confined in vacuum in electromagnetic traps (*1*), single-molecule spectroscopy of molecules in solid matrices (*2*), and the detection of molecules on surfaces with high spatial resolution by near-field scanning optical microscopy (*3*). These techniques are based largely on observation of the fluorescent emission from the molecule during repeated photonic excitation events and provide information about energy levels and the environment of the molecule. We report single-molecule detection (SMD) for an electroactive molecule in solution as it repeatedly undergoes electron-transfer reactions at an electrode held at a small distance from a counterelectrode in a scanning electrochemical microscope (SECM) (*4*, *5*).

The principle of this experiment is illustrated in Fig. 1. To achieve SMD in the SECM, a small tip electrode of nanometer dimensions and with a geometry that provides confinement of the molecule near the active tip area is held near (~10 nm) a conductive substrate. The solution concentration is adjusted so that, on average, only a single molecule will reside in the volume defined by the tip area and tip-substrate spacing d. Consider a tip of radius $a = 5$ nm held at $d = 10$ nm. For a 2 mM solution of an electroactive species, it is probable that only one molecule will be present in the $\sim 10^{-18}$ cm^3 volume beneath the tip (*5*). The time required for the molecule to transit between tip and substrate is of the order of $d^2/2D$, where D is the diffusion coefficient of the molecule. Thus, a molecule with $D = 5 \times 10^{-6}$ cm^2/s will transit the gap in about 100 ns or undergo ~10^7 round trips between tip and substrate per second. If an electron-transfer event occurs at each collision with the tip, a current of the order of 1 pA will flow. In this case, SMD depends on the 10^7 amplification factor provided by the positive feedback of the SECM. The molecule is confined to the space below the tip because the conductive tip is slightly recessed below the large insulating sheath that surrounds it, as shown in Fig. 1. Further axial confinement of a charged species might be afforded by the electric field in the gap.

For the initial test of SMD by SECM we chose [(trimethylammonio)methyl] ferrocene (Cp_2FeTMA^+) as the electroactive molecule, because both this species and its oxidized product are stable in aqueous media and undergo rapid heterogeneous electron-transfer reactions at electrodes in a convenient range of potentials. Solutions contained 2 mM Cp_2FeTMA^+ with $NaNO_3$ as the supporting electrolyte. In all of the experiments, an indium-tin oxide (ITO, Delta Technologies, Stillwater, New York) electrode was used as substrate. The tip was fabricated from an electrochemically sharpened 125-μm Pt-Ir (80%-20%) wire coated with Apiezon wax or polyethylene glue. We exposed the end by placing the tip in a scanning tunneling microscope (STM) and allowed it to approach the ITO substrate until a set-point current (0.5 nA) began to flow. By constructing the tip in this manner, we ensured that the tip and its insulating sheath would approach the ITO surface perpendicularly without alignment difficulties. Details of the fabrication of these tips and their characterization are given elsewhere (*5*–*7*). The instrument used in these studies has been described in (*8*, *9*) and is capable of both STM and SECM measurements with a vertical (z direction) resolution of better than 1 Å and a current sensitivity as low as 50 fA when the proper filter is used. The electrochemical cell contained a Pt counterelectrode and either a saturated calomel electrode (SCE) or a Pt quasi-reference electrode.

The correct tip geometry is essential for the successful trapping of a molecule. Information about the exposed area of the tip and the shapes of the tip and insulating sheath can be obtained from electrochemical measurements, that is, from determination of the tip current i_T as a function of d as the tip is moved toward the substrate in an SECM (*7*). All of the tip currents reported were corrected for the background current in the blank solution, that is, a solution containing only supporting electrolyte, at large d. A typical approach curve of this type taken with a solution of 2 mM Cp_2FeTMA^+ and 2.0 M $NaNO_3$, with the tip held at 0.55 V versus SCE where Cp_2FeTMA^+ oxidation is diffusion-controlled, is shown in Fig. 2. The ITO substrate was biased at −0.3 V versus SCE, so that Cp_2FeTMA^{2+} generated at the tip was rapidly reduced back to Cp_2FeTMA^+ at the ITO surface. The exposed radius a can be found (*5*) from the steady-state current $i_{T,\infty}$, when the tip is assumed to be a disk-shaped

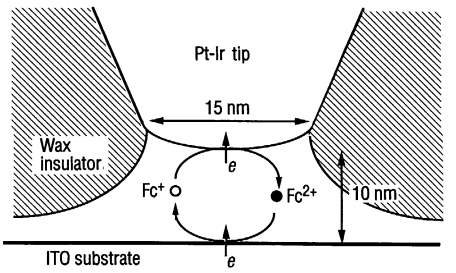

Fig. 1. Idealized schematic illustration of the tip geometry and the tip-substrate configuration used.

Department of Chemistry and Biochemistry, University of Texas, Austin, TX 78712, USA.

*To whom correspondence should be addressed.